Journal of Marine Science and Technology (2022) 27:887–906
https://doi.org/10.1007/s00773-022-00878-6

ORIGINAL ARTICLE

Identification of the geometric design parameters of propeller blades from 3D scanning

Eirik B. Njaastad[1] · Sverre Steen[2] · Olav Egeland[1]

Received: 7 September 2021 / Accepted: 6 February 2022 / Published online: 7 March 2022

Abstract

This paper presents a new method for the identification of geometric design parameters of ISO 484 class propeller blades from scanned point cloud data. The method can be used for tolerance inspection and in-line measurement of manufactured blades, and for wear assessment and reverse engineering of propellers in service. The geometry of the propeller blades is specified by a set of blade sections stacked radially on concentric cylindrical surfaces. For each of these sections, the chord line and mean camber line is determined, and geometric design parameters such as the pitch, skew, chord length, camber, and thickness distributions are identified. The proposed method is a complete procedure for identifying the design parameters of marine propeller blades from point cloud data, and includes a novel method for the precise identification of the mean camber line based on Voronoi diagrams and Delaunay triangulation. The paper includes validation of the proposed method in experiments where reverse engineering is applied to a propeller blade of the KVLCC2 propeller, and in 3D scanning of a large, high-skew thruster blade where the results were compared to CMM measurements.

Keywords Blade inspection · Propeller geometry · Reverse engineering · Scanned point cloud

List of symbols

α_h	Geometric pitch angle near the hub
α_t	Geometric pitch angle near the tip
α	Geometric pitch angle
P	Pitch distance
D	Propeller diameter
R	Propeller radius
r	Radius of a propeller section
r_t	Radius near the tip
r_h	Radius near the hub
l	Chord length
f	Camber distribution
f_0	Maximum camber
t	Thickness distribution
t_0	Maximum thickness
i	Rake
θ_s	Skew angle of a propeller section
θ_{sp}	Skew angle of propeller
LE	Leading edge
TE	Trailing edge

✉ Eirik B. Njaastad
eirik.njaastad@sintef.no

[1] Department of Mechanical and Industrial Engineering, Norwegian University of Science and Technology (NTNU), 7491 Trondheim, Norway

[2] Department of Marine Technology, Norwegian University of Science and Technology (NTNU), 7491 Trondheim, Norway

1 Introduction

The surface profile of a propeller blade has a vital impact on the efficiency of the propeller. It is, therefore, important that accurate measurement techniques are available in the manufacturing of high-performance marine propellers. Evaluation of the geometric errors is typically carried out through the various stages of the production process and for the final inspection of products. Due to the highly complex surface geometry of the propeller blades, inspection is often time-consuming and involved.

Coordinate measuring machines (CMM) are typically used for propeller inspection where discrete points on the surface are sensed with a probe. Since the measurements are conducted pointwise, the efficiency of CMM inspection is relatively low. Propeller manufacturing is often characterized by small batch production with frequent changes in product dimensions, which means that time-consuming programming and set-up of coordinate measuring machines

must be carried out frequently. CMM inspection processes can also be challenging to integrate with other automated production processes, such as robotic grinding or polishing. Consequently, it is interesting to consider alternative inspection methods that are potentially less time-consuming, less expensive, fully automatic, and still offer an adequate level of accuracy.

Optical measurement technologies have proved increasingly applicable for the inspection of manufactured parts. For marine propeller blades, optical measurement systems offer several advantages. The planning and programming of an inspection task can be simplified, and by quickly and efficiently collecting a massive number of data points from the surface of the part, the time required to inspect a manufactured propeller can be significantly reduced. Optical systems of small size can be used in combination with an industrial robot for inspection of large products, which is interesting for flexible integration in automated production systems.

A variety of methods for optical measurement of propeller blade geometry has previously been proposed and studied. Almost three decades ago, Golini [1] proposed using a profilometer to measure the shape of a propeller blade. The system was capable of recording ten measurements per second using laser interferometry. Menna and Troisi [2] studied the possibility of using various low-cost approaches based on photogrammetry and laser scanning for generating complete and accurate 3D CAD models of small propellers. Zhang and Lu [3] proposed a solution for measuring the width of marine propellers using parallel axis stereo vision. Focus variation, a technique mainly used for measuring geometrical defects such as surface waviness and roughness, gave 3D depth readings. As proposed by Abdullah et al. [4], this method could also be used to evaluate geometric and dimensional defects of small propeller blades. Cavada and Fadón [5] gave a thorough assessment of various laser-based techniques for measuring marine propellers. Both direct measurements with laser and combinations of laser measurement and surface probing were considered. Beng and Choong [6] used an unspecified type of 3D scanner and computer-aided design software to characterize the geometry of a small outboard marine propeller. It is worth mentioning that other sectors of the shipbuilding industry also see potential applications of optical inspection methods. Examples of this include the as-built measurement of prototype ship design [7] and reverse engineering of hull design for energy efficiency evaluation [8]. Reverse engineering of an old propeller is described by Hand et al. [9], where structured light and coherent laser radar scanning sensors were used to recreate the propeller of a ship constructed during the American Civil War.

A marine propeller blade is, in principle, a rotating airfoil that produces thrust. Airfoils are also found in fans, compressors, and turbines, which makes it relevant to consider studies on optical blade inspection for other sectors. These studies include extraction of the sectional foil curves [10], reconstruction of mean camber line [11], leading edge and trailing edge localization [12], shape matching [13], and position and orientation error evaluations.

There exist some challenges for optical measurement techniques when applied to the inspection of marine propellers. Difficulties with highly reflective surfaces, requirements for unobstructed line of sight, imprecise stitching when joining results from multiple scans, and lack of structure in the resulting point clouds are all examples of these challenges. However, the benefits of the rapid non-contact acquisition of dense spatial measurements have outweighed these difficulties and inspired continued advancement.

To extract the required design parameters of the propeller blades, precise and efficient processing of the massive amount of data arising from optical 3D scanning is necessary. Several efforts have previously addressed and studied the problem of identifying the most decisive design parameters of propellers from scanned data. Patrikalakis and Bardis [14] presented a set of algorithms for the extraction of gross geometrical features of marine propeller blades represented in terms of B-spline surfaces. Their approach for camber line calculation requires an involved integration of a system of differential equations along with a complicated error evaluation scheme. Jinkerson et al. [15] extended the work of [14] with useful methods for unconstrained and constrained localization and feature extraction for propellers. Their method requires a non-uniform rational basis spline (NURBS) representation of the blade geometry in addition to a set of corresponding spatial point measurements of the manufactured blade surface. The authors also state that tedious and manual preprocessing of the measured data points is necessary for the localization methods to succeed. Allen et al. [16] proposed an approach to this problem where the measured point clouds were converted into a surface representation of the blade, and performed a series of NURBS curve interpolations. As for the methods in Ref. [15], the approach requires accurate NURBS representation of the blade geometry and, in addition, the computation of the signed deviation from the design surface for each measured point. More recently, Yeo and Choong [6] characterized the design parameters for a small outboard marine propeller. However, their method is also based on interpolating a CAD model of the scanned data, which is a complicated step that is prone to errors and involves several manual steps.

To correctly identify the propeller design parameters, a set of particular sectional curves need to be precisely extracted. Intermediate surface or mesh reconstruction steps will introduce an interpolated and imprecise surface, which effectively reduces the accuracy of the inspection of a point by taking in point deviations from connecting surface patches. Direct slicing and identification of the foil sections

from the point cloud data would therefore increase the accuracy of the inspection methods, by rejecting the influence from measurement deviations in the regions close to each point. Li et al. [17], Kostas et al. [18], and several others have proposed airfoil models that can be used to reconstruct airfoils and hydrofoils from possibly noisy measurements of foil sections. A comprehensive survey and comparison of airfoil shape parameterizations are given by Masters et al. [19]. Consistent reconstruction of surfaces and boundary curves requires that the measured points take the form of organized point clouds, which is not straightforward to achieve for standard optical measurement techniques.

The geometric shape of propeller blades can be approximated by parametric blade models, commonly employed for parametric design studies and performance optimization. Several parametric propeller blade models have been proposed in the literature, and a recent example is the work of Arapakopoulos et al. [20]. An alternative approach to the problem of identifying the design parameters from scanned data could be to set up and solve a minimization problem, where the deviation between a parametric model and a scanned point cloud of a blade is minimized. However, solving such a minimization problem for the large amount of data generated from 3D scanning is computationally intensive.

In this paper, we propose a new method for the identification of the propeller design parameters using point cloud data originating from 3D cameras. The main idea of the proposed method is to extract the sectional contours of propeller blades directly from the point cloud and to determine the mean camber line, the leading and trailing edges, and the chord line for each of the sections. The identification of these parameters allows for the determination of the original design parameters of the propeller with high precision. The success of the approach is subject to the accuracy of the camber line determination step, which we will cover in detail. Emphasis has been placed on complying with the globally recognized standard for marine propeller tolerances, ISO 484.

The performance of the approach is validated in experiments where reverse engineering is performed for a propeller blade of the KVLCC2 design. Further validation is performed where we identify the design parameters of a large, high-skew propeller blade from a 3D scanning of its surface, using the ATOS ScanBox developed by GOM, and compare the results with the actual propeller design data and CMM measurements.

The organization of the paper is as follows: Sect. 2 discusses the geometry and representation method of marine propellers and gives an overview of the ISO 484 standard. The proposed method for extracting the sectional curves of the propeller blade is presented in Sect. 3, where a discussion on mean camber line determination is included. Case studies and results are presented in Sect. 4. Finally, conclusions and suggestions for further work are given in Sect. 5.

2 The geometry of marine propellers

This section presents a formalism for the description of marine propeller geometry based on [21]. A global reference frame (X, Y, Z) is defined, as shown in Fig. 1, where the origin is in the center of the propeller hub. The X-axis is along the propeller shaft in the forward direction of the vessel. The Y-axis is positive toward the port side, and the positive Z-axis is pointing in the vertically upward direction of the vessel. In addition, the local reference frame (x^r, y^r, z^r) is defined as a body-bound frame rotating about the X-axis. A typical marine propeller will have three to six blades attached to a boss or hub, which in turn is mounted on the propeller shaft. Each propeller blade is defined relative to a propeller reference line, which is fixed in the blade with direction normal to the propeller shaft. There is one propeller reference line for each blade. In the description of a propeller blade, the z^r axis of the local reference frame can be aligned with the propeller reference line of the blade.

The quantities that define the overall propeller geometry are its diameter, pitch, pitch distribution, chord length distribution, number of blades, camber distribution, and thickness distribution. Additional parameters of importance are the skew and rake of the propeller and the diameter of its hub.

Propeller diameter

The diameter D of a propeller is defined as the diameter of the circle it spans while rotating, seen directly from the back of the vessel. This concept is relatively straightforward for

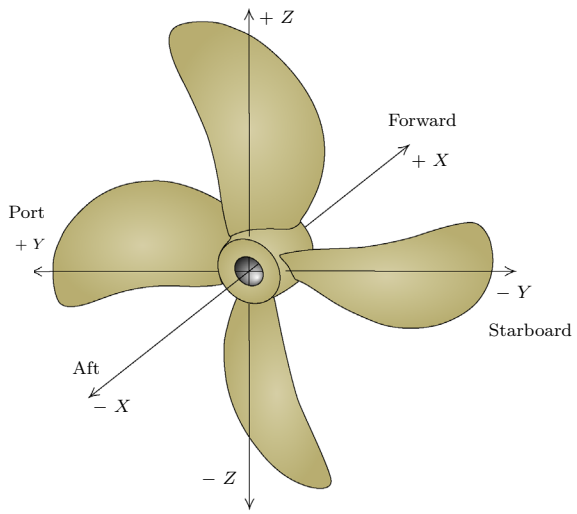

Fig. 1 Global reference frame. The X axis is along the propeller shaft in the forward direction

propellers with fixed pitch. For some classes of propellers, the controllable pitch propellers (CPP), however, the spanning circle will vary depending on the mechanically varied pitch of the blades. In this case, the concept of a design pitch is practiced. The diameter of a CPP is then determined by orienting the propeller blade, such that the specified blade section pitch is equal to the design pitch. Figure 2 illustrates the propeller diameter and accompanying radius.

Pitch and pitch distribution

The propeller pitch is the theoretical distance P a propeller will move forward in a solid medium for each rotation, not allowing for slip. The distance is illustrated in Fig. 3. The pitch of a blade section can also be defined as an angle. The relation between the pitch distance P and the pitch angle α is given by

$$\alpha = \arctan\left(\frac{\mathrm{P}}{2\pi r}\right). \tag{1}$$

Typically, the propeller blades are twisted to achieve almost constant pitch of the blades from root to tip. To describe this twist, a pitch distribution P(r) is given, where r is the radius considered. The relationship between pitch angle and pitch distribution can then be expressed as

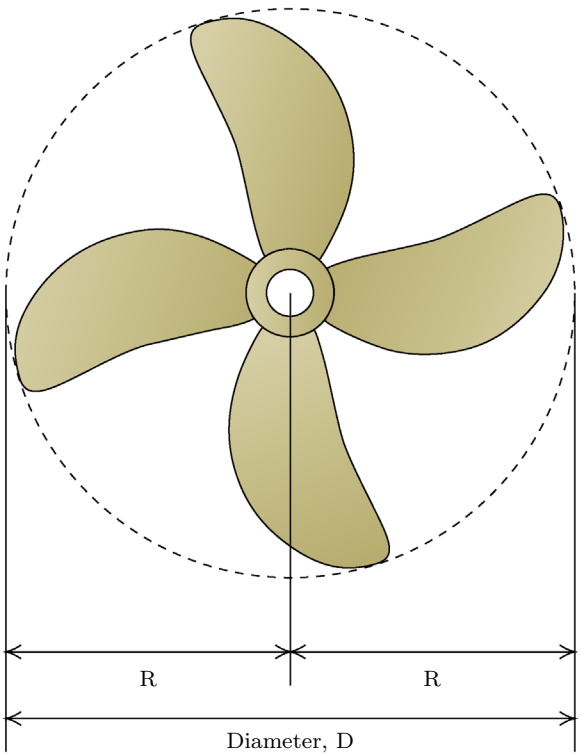

Fig. 2 The diameter D is the most apparent feature of any propeller and is simply the circular extent that the extreme tips of the propeller blades span as the propeller rotates

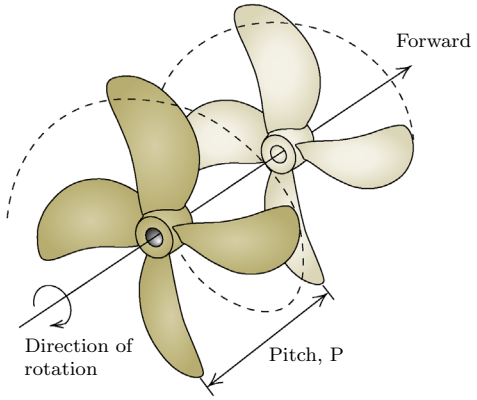

Fig. 3 The propeller pitch P is the theoretical linear distance a propeller travels during a complete rotation

$$\alpha = \arctan\left(\frac{\mathrm{P}(r)}{2\pi r}\right) = \arctan\left(\frac{\mathrm{P}(\rho)}{2\pi\rho\mathrm{R}}\right), \tag{2}$$

where $\mathrm{R} = \mathrm{D}/2$ is the propeller radius and ρ is the non-dimensional radius defined by

$$\rho = \frac{r}{\mathrm{R}}. \tag{3}$$

Figure 4 illustrates the geometric relationship between the pitch distance and angle for a blade section near the hub, and a section near the tip of the blade. The pitch angle α will typically be decreasing with increasing radius to keep the pitch distance P nearly constant. It is common to refer to the pitch located at 70% of the total propeller radius, which is at $\rho = 0.7$.

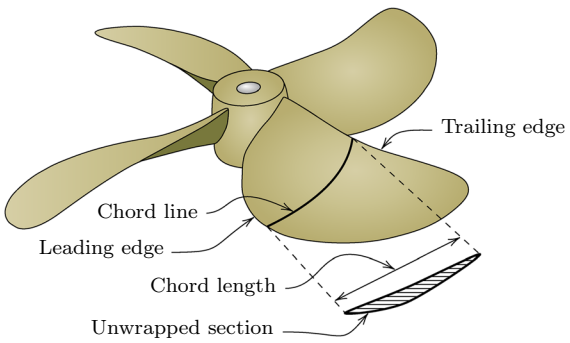

Fig. 4 The relation between propeller pitch distance P and angle for a propeller blade section near the hub r_h and a section near the tip r_t of the blade. The geometric pitch angle α spans between a line perpendicular to the propeller axis of rotation and a pitch reference line at each blade section. Each pitch reference line may pass through the leading and trailing edges of the section

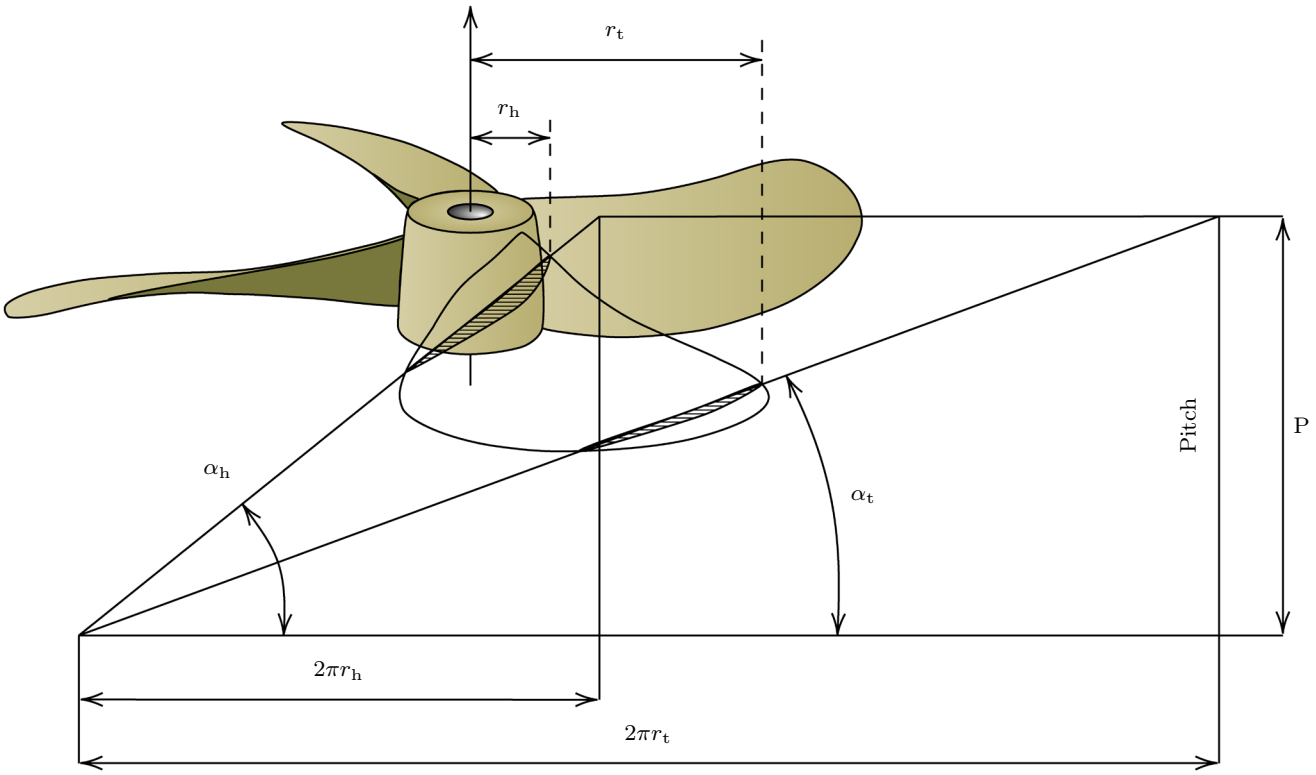

Fig. 5 The geometry of propeller blades is defined from a set of radial sections. A chord line runs through each section from the leading edge (LE) to the trailing edge (TE). The length of the chord line is called the chord length

Cylindrical foil sections

The geometry of a propeller blade is described by selecting a set of N values $\rho_1, \rho_2, \ldots, \rho_N$ for the non-dimensional radius $\rho = r/\mathrm{R}$. Then, the geometry of the propeller blade is given by the N cylindrical cross sections of the blade at the non-dimensional radii $\rho = \rho_i$, where the cylindrical cross sections are concentric with the propeller axis. At each considered radius, the propeller blade has a different cross section representing the distribution of pitch, thickness, and other design parameters. Figure 5 illustrates how a cylindrical propeller section resembles the cross section of a foil.

Let the z^r-axis of the rotating local reference frame be along the propeller reference line of the blade. To describe the foil parameters of the blade, the cylindrical sections are unwrapped onto a planar surface parallel to the $x^r y^r$ plane of the local reference frames, as shown in Fig. 6.

The unwrapped blade sections are also termed expanded blade sections. The shape of the unwrapped blade sections is defined by the geometric foil parameters such as thickness, camber, chord length, and the leading and trailing edges. Figure 7 shows the unwrapped foil, with the main terminology used for describing the foil sections. Precise identification of the leading edge (LE) and trailing edge (TE) is necessary for determining the chord line and hence the center point of the blade section. The blade reference line, which is plotted for the expanded blade in Fig. 6, is the line through the midpoint of the camber line of the sections.

Chord length distribution

At a given radius, the leading and trailing edges are connected via a helical line segment, called the chord line. For the unwrapped sections, the chord line becomes a straight line and is also called the nose-to-tail line. The length of the chord line is termed the chord length l, as shown in Fig. 7. The chord length distribution $l(r_i)$ is a set of chord lengths at predefined sections of a propeller blade at $r = r_i = \rho_i \mathrm{R}$.

Through the chord length distribution, the unfolded blade area of the propeller can be expressed as

$$A_E = \mathrm{Z} \int_{r_0}^{\mathrm{R}} l(r)\mathrm{d}r, \tag{4}$$

where Z is the number of blades, r_0 is the radius of the root section, and R is the propeller radius. The blade area is a parameter that affects the propeller's efficiency and thrust to a large extent.

The midpoint of the chord line is called the mid-chord, and is commonly used for defining the skew and rake of each propeller blade section.

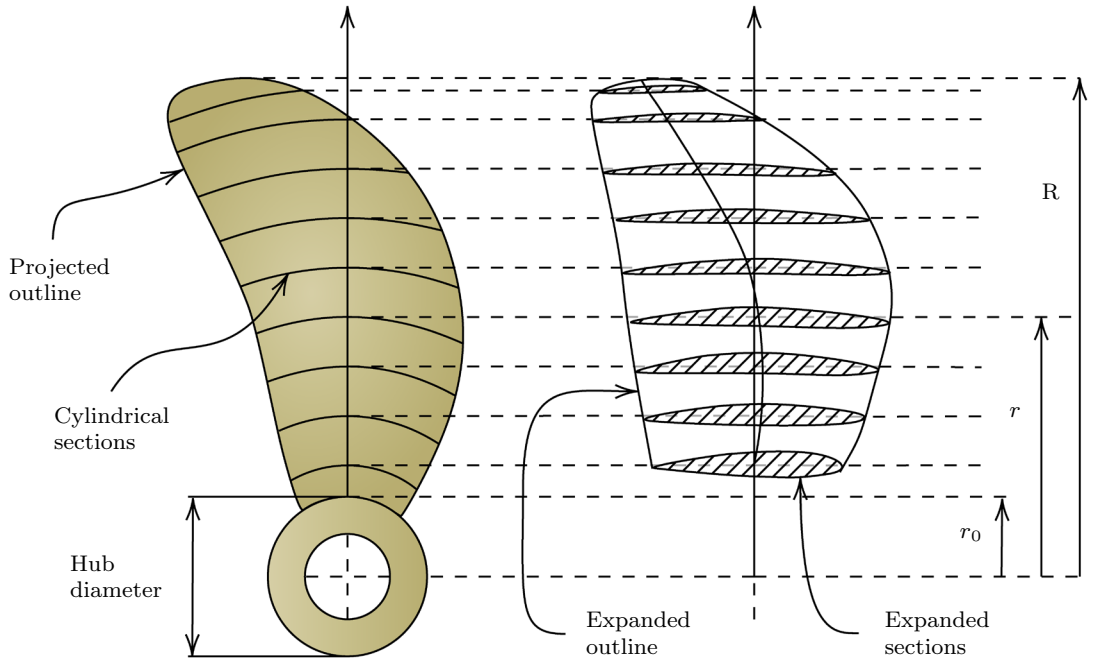

Fig. 6 Unwrapping the radial sections. The original cylinder sections of a propeller blade at various radii are shown to the left. The respective sections defined along a flat plane are shown to the right. R is the total propeller radius, r is the radius of an arbitrary blade section, and r_0 is the hub radius of the propeller

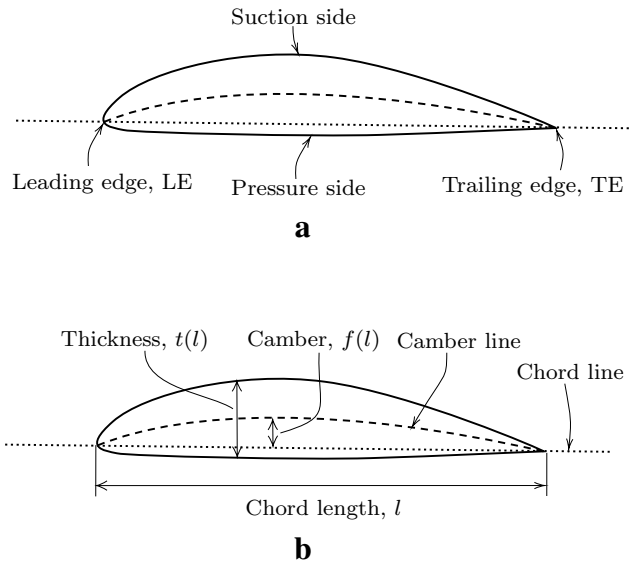

Fig. 7 Definition of section thickness, chord line, chord length, camber, and camber line in **b**. The blade suction and pressure side, along with its leading edge (LE) and trailing edge (TE) in **a**

Camber and thickness distribution

The chord line divides the blade section into an upper and lower surface. If we trace the midpoints between the upper and lower surfaces, we get a curve called the mean camber line. The distance between the chord line and the mean camber line is called the camber of the section. In Fig. 7, the concepts of the camber and mean section camber lines are illustrated. A camber distribution $f(l)$ can be developed by measuring the camber at several points along the chord line of a section. The camber is then measured orthogonal to the chord line. The camber ratio is expressed as

$$\mathrm{C} = \frac{f_0}{l} \tag{5}$$

where f_0 is the maximum camber, and l is the chord length of the foil section.

The thickness distribution $t(l)$ specifies the distance between the pressure and suction sides of a blade at points along the chord line, as illustrated in Fig. 7. The maximum thickness t_0 is usually between 1/3 and 1/2 chord lengths from the leading edge.

Skew and rake

The skew angle $\theta_s(r)$ of a particular section is the tangential component of the angle formed on the propeller blade between the propeller reference line (z-axis) and a radial line from the propeller origin, passing through the mid-chord of the considered section at radius r. The purpose of a skewed shape is to avoid cavitation while maintaining propeller efficiency [21]. The centerline of each blade is then swept curvilinearly backward of the direction of rotation, and as a result, the contour of the blade is not radially symmetric around its centerline. The asymmetrical contour of a skewed propeller blade is shown in Fig. 8. The propeller skew angle θ_{sp} is the largest spanning angle between two lines from the propeller origin running through the various mid-chords of the radial blade sections.

For a given foil section at radius r, the skew can be expressed as

$$S = \frac{r\theta_s(r)}{\cos(\alpha)}, \tag{6}$$

where $\theta_s(r)$ is the skew angle, and α is the pitch angle for the considered foil section. The propeller skew can be divided into forward and aft skew. A propeller for which the blades are swept in the direction of rotation is said to have forward skew. An aft skewed propeller has blades swept opposite of the direction of rotation. These concepts are illustrated in Fig. 8.

Propeller rake is defined as the displacement of the radial foil section along the shaft or x-axis. Displacements in the aft direction are considered as a positive rake, and the rake measured at the blade tip is frequently used as a rake measure. The rake comes from two components, namely the initial rake i_{in} and the skew-induced rake i_s. The total rake i_{tot} is then

$$i_{tot} = i_{in} + i_s. \tag{7}$$

The skew-induced rake is an axial displacement caused by the skew imposed on a blade section. For a given skew angle $\theta(r)$ and pitch angle α, the skew-induced rake can be determined by

$$i_s = \theta_s(r)\tan(\alpha)r. \tag{8}$$

In Fig. 9, the relation between the pitch, skew, and types of rake impacting a propeller blade section is illustrated. The figure also shows how the chord line and the mid-chord is central in determining these parameters.

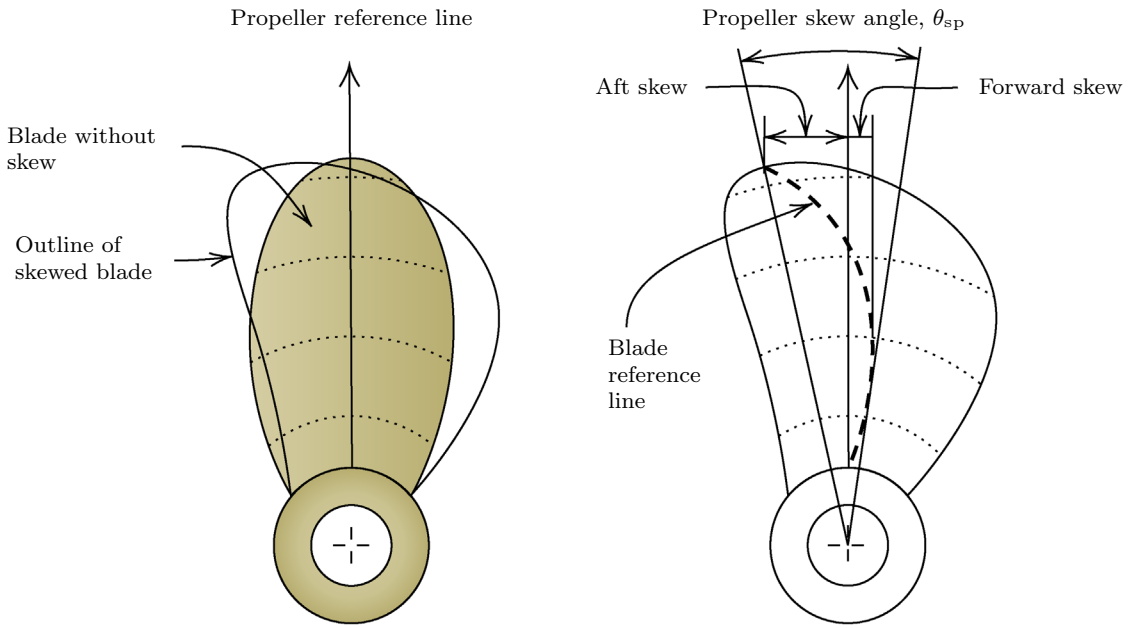

Fig. 8 The left figure outlines a skewed propeller blade and a blade without skew relative to a common propeller reference line. The difference between aft- and forward skew is shown to the right, with the blade reference line marked

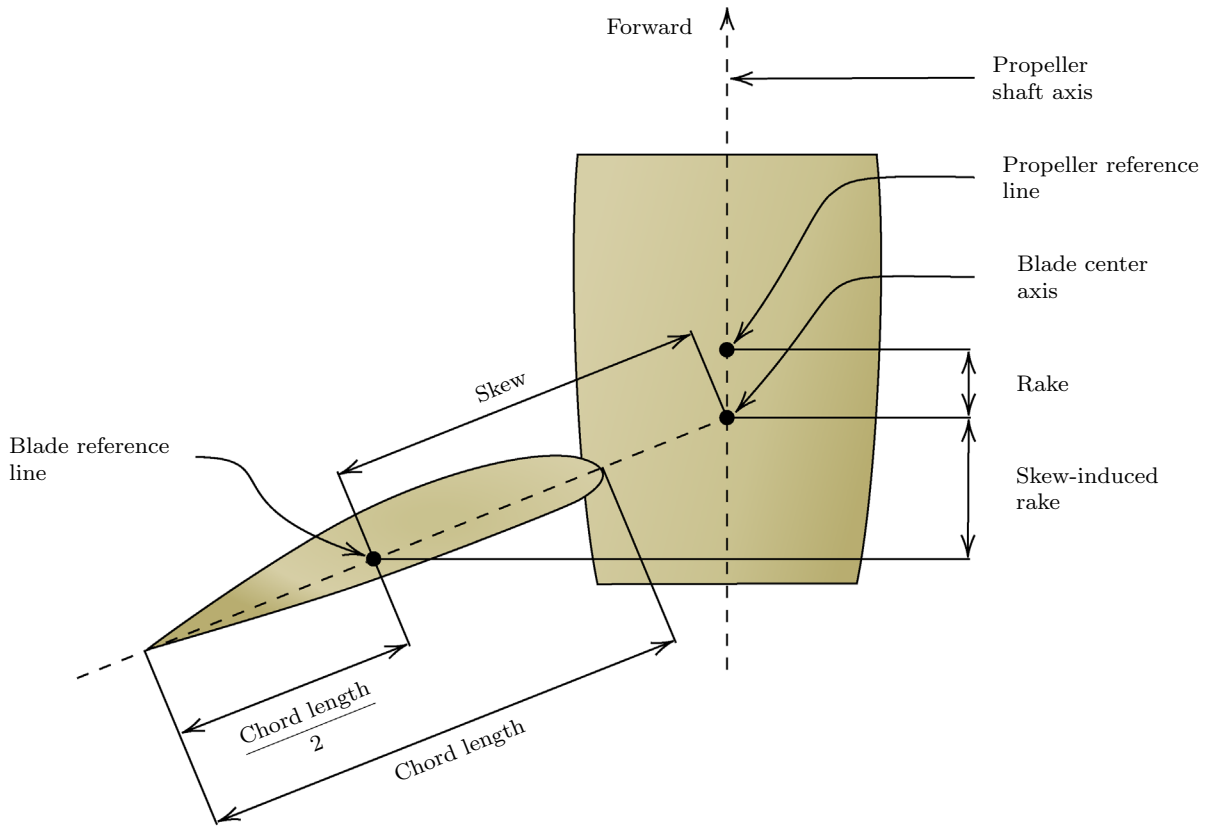

Fig. 9 The relationship between the propeller shaft axis, the propeller reference line, the blade reference line, and the blade center axis for each of its blades. Note how skew and rake affect the distance between the mentioned axes

2.1 ISO 484

Marine propellers are almost exclusively manufactured, repaired, inspected, and certified according to the International Standard ISO 484 from 1981. The standard has four tolerance classes, regulating different levels of manufacturing accuracy. When a propeller is inspected, vital measurements are made on each blade of a propeller at specified radii from the propeller axis. Most often, these measurements are conducted at: some radii near the hub, then at the non-dimensional radii 0.4, 0.5, 0.6, 0.7, 0.8, 0.9, and 0.95. For each of the radii, the blade surfaces are measured at a set of prescribed points. ISO 484 explicitly specifies tolerances on the propeller design pitch, pitch distribution, extreme radius of the propeller, thickness distribution, blade surface roughness, and static unbalance. Also, the standard describes the required accuracy of the measuring equipment used for inspection.

Cavada and Fadón [5] pointed out that manually operated measurement systems, where various points on the propeller's surface are measured by direct probing, are generally not accepted by the classification societies, as inspection of the exact points defined by the ISO 484 standard cannot be guaranteed.

3 Overview of the proposed method

In this section, our proposed method is presented. The objective is to develop a fully automated approach for deriving geometric design parameters from a given point cloud. The fundamental idea of this paper is as follows. First, we extract the radial sections of a propeller blade directly from scanned point cloud data and transform them into a corresponding planar surface. Then, the foil geometry parameters are identified for each radial section by interpolating the boundary curve and finding the mean camber line, which is found by generating the Voronoi diagram and Delaunay triangulation of the section points. The identified geometric parameters are compiled, and the overall design parameters

of the propeller are developed. The success of the approach depends on the accuracy of the identified foil geometry parameters for each section, with particular stress on accurately locating the mean camber line and leading and trailing edges. Because the data points generally have uneven distribution and are noisy, systematically locating said parameters is a challenging task. Another prerequisite for successful identification is that the propeller or propeller blade is oriented correctly according to its datum.

3.1 Section extraction and unwrapping

For each of the selected radial sections, we construct a cylindrical surface of radius r equal to the considered radius and select all points coinciding with it. Since only few points are at the exact radial distance, all data points within a user-defined distance of δ from the sectional cylinder surface are radially projected onto the cylinder surface. In the propeller-fixed local reference frame, the selected points (x^r, y^r, z^r) have to fulfill the following condition:

$$r - \delta \leq \sqrt{(y^r)^2 + (z^r)^2} \leq r + \delta, \tag{9}$$

This results in a set of n_i points (x_i^r, y_i^r, z_i^r), $i = 1, \ldots, n_i$ for each radius $r_i = \rho_i \mathrm{R}$.

As described in the previous section, it is necessary to unwrap the radial sections onto a planar surface parallel to the xy plane of the local reference plane to identify the various foil parameters. In other terms, we need to perform a transformation that preserves distances between points. A point (x^r, y^r, z^r) laying in the extracted radial section with coordinates in the local reference frame will have coordinates (x, y, z) in the unwrapped planar section where

$$x = x^r, \tag{10}$$

$$y = \arctan2(y^r, z^r)\sqrt{(y^r)^2 + (z^r)^2} \tag{11}$$

$$z = r. \tag{12}$$

The transformation between radial and flat sections is illustrated in Fig. 6.

3.2 Interpolation of unwrapped boundary curves

Following the extraction and unwrapping of the blade sections, we now have a set of unorganized and potentially noisy points representing each of the selected radii r_i. To be able to identify the leading and trailing edges, but also the thickness distribution and other essential parameters, we need to interpolate a boundary for each of the sections. With coordinates given by (10)–(12), the sets of unwrapped points are separately located in planes at the given radial distances from the datum, which means that finding the sectional parameters for a given radius r_i becomes a two-dimensional problem.

For each radius r_i, we downsample the set of points $\mathbf{p}_j = [x_j, y_j]^{\mathrm{T}}$, $j = 1, \ldots, n$ by dividing them into an integer grid G. Then, all points that fall into the same cell D of the grid are replaced by one new point in D. The cells D are rectangles with two sides l_1 and l_2, such that its height is l_1 and its width is l_2. The output of the downsampling process is a new set $\mathbf{p}_k$ of m points, where $m \leq n$.

Next, we sort the sampled points $\mathbf{p}_k$ for each of the sections according to the angle ϕ_k which is formed between the positive x axis and the rays to each of the points in the plane as

$$\phi_k = \arctan2(p_{kx} - \bar{p}_x, p_{ky} - \bar{p}_y), \tag{13}$$

where $\bar{\mathbf{p}} = [\bar{p}_x, \bar{p}_y]^{\mathrm{T}}$ is the centroid given by

$$\bar{\mathbf{p}} = \frac{1}{m}\sum_{k=1}^{m} \mathbf{p}_k. \tag{14}$$

Given a sampling grid of reasonable resolution, the downsampled and sorted points now form a boundary that represents the foil section at each of the selected radii. The boundary curve can be described parametrically as

$$L(s_i) = (x(s_i), y(s_i)), \tag{15}$$

where $s_i \in \{s_0, \ldots, s_m\}$ are called the breakpoints. The breakpoints of the boundary curve are not necessarily uniformly distributed, resulting in an unbalanced effect on the subsequent identification of the camber line. Therefore, a piecewise linear interpolation is used, which gives

$$\begin{cases} x(s) = (x_{k+1} - x_k)s + x_k \\ y(s) = (y_{k+1} - y_k)s + y_k \end{cases} \tag{16}$$

for $s \in [s_k, s_{k+1}]$ and $k = 0, 1, \ldots, m-1$. This gives a continuous interpolated boundary curve

$$L(s) = (x(s), y(s)). \tag{17}$$

3.3 Voronoi diagrams

All propeller foil sections may be regarded as a thickness distribution symmetrically superimposed upon a mean camber line. Consistent and accurate identification of the camber line is required to obtain the foil parameters robustly. A method for characterization of the line should be robust to noise and various realizations of the foil features.

We propose an approach to this where Voronoi diagrams and Delaunay triangulation [22–24] are introduced in the characterization of ship propellers based on point cloud data.

First, the basics of Voronoi diagrams are presented. Consider a set S of n sites $\mathbf{p}_1, \ldots, \mathbf{p}_n \in \mathbb{R}^2$, which are points in the plane. Then, the set of points

$$B(\mathbf{p}_i, \mathbf{p}_j) := \{\mathbf{p} \in \mathbb{R}^2 \mid \|\mathbf{p} - \mathbf{p}_i\| = \|\mathbf{p} - \mathbf{p}_j\|\} \tag{18}$$

will form the perpendicular bisector of the sites p_i and p_j, which are the points of equal distance to the two points or sites. This bisector divides the plane into two open half planes $H(\mathbf{p}_i, \mathbf{p}_j)$ and $H(\mathbf{p}_j, \mathbf{p}_i)$, where

$$H(\mathbf{p}_k, \mathbf{p}_l) := \{\mathbf{p} \in \mathbb{R}^2 \mid \|\mathbf{p} - \mathbf{p}_k\| < \|\mathbf{p} - \mathbf{p}_l\|\}, \tag{19}$$

is the open half plane of points that are closer to the site $\mathbf{p}_k$ than the site $\mathbf{p}_l$. The intersection of all the half planes $H(\mathbf{p}_i, \mathbf{p}_j)$ for $j = 1, \ldots, n$ will be the set of points that are closer to the site $\mathbf{p}_i$ than any other site in the set S. This set of points is called the Voronoi cell

$$R(\mathbf{p}_i, S) := \bigcap_{\mathbf{p}_j \in S,\ i \neq j} H(\mathbf{p}_i, \mathbf{p}_j). \tag{20}$$

of the site $\mathbf{p}_i$. A Voronoi cell forms a convex region bounded by a set of at most $n - 1$ connected line segments. The union of all the Voronoi cells is the Voronoi diagram Vor(S).

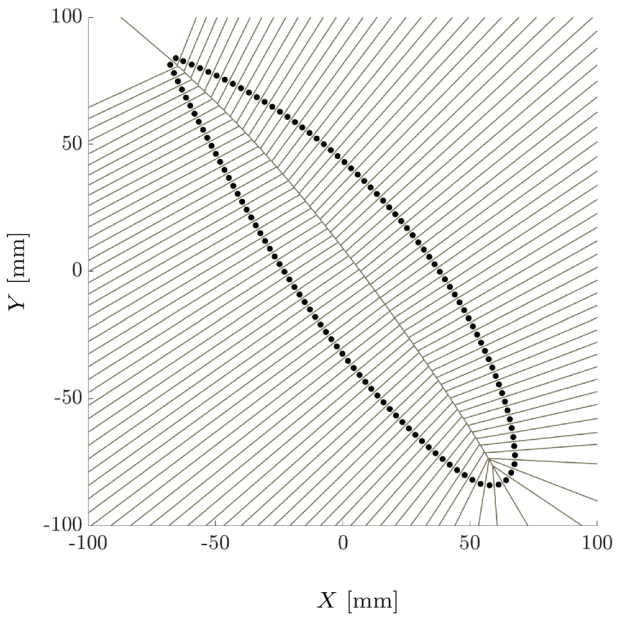

Fig. 10 A Voronoi diagram where the sites are on the boundary curve of a propeller blade section. The mean camber line is approximated by Voronoi edges between one site at the pressure side and one site at the suction side

The line segments forming the boundaries of a Voronoi cell are referred to as Voronoi edges, whereas the endpoints of these edges are called Voronoi vertices. Two Voronoi cells with a common Voronoi edge are said to be Voronoi neighbors. An illustration showing a Voronoi diagram for a blade section is given in Fig. 10.

3.4 Mean camber line from Delaunay triangulation

Delaunay triangulation [24] is closely related to Voronoi diagrams. Given a Voronoi diagram Vor(S), a Delaunay triangulation DT(S) is established by connecting the sites $\mathbf{p}_i$ of neighboring Voronoi cells with straight lines which are called Delaunay edges. These Delaunay edges form a set of faces that are called Delaunay triangles. The aggregate of these Delaunay triangles is the Delaunay triangulation DT(S), which tessellates the area defined by the set of points S.

Let the Delaunay triangle T_{ijk} be the triangle where the corners are the three sites $\mathbf{p}_i, \mathbf{p}_j, \mathbf{p}_k$ of the Voronoi diagram. Then, the circumcircle of T_{ijk}, which is the circle that passes through the three corners of T_{ijk}, will not contain any other site of Vor(S). Moreover, the center $\mathbf{q}_{ijk}$ of the circumcircle of T_{ijk} is the Voronoi vertex within the triangle.

The usefulness of Delaunay triangulation in connection with the identification of foil section parameters is that the mean camber line can be found efficiently and accurately from the measured points $L(s_i)$ on the boundary curve. It is then used that the center $\mathbf{q}_{ijk}$ of the circumcircle of the triangle $T_{ijk} \in DT(\mathbf{p})$ is at the Voronoi vertex of the sites constituting the corners of the triangle. The Voronoi vertex will be at equal distance from the three corners of T_{ijk}. This means that the points $\mathbf{q}_{ijk}$ will have equal distance δ_d to the pressure and suction side of the boundary curve. Note that this distance is measured along a line that is normal to the boundary curve. The thickness of the foil section can then be approximated by $t_d = 2\delta_d$.

The mean camber line is typically defined such that the distance δ_c to the boundary curve is the same on the suction side and the pressure side, where δ_c is measured along a line that is normal to the mean camber line, and where $t = 2\delta_c$ is the thickness of the foil section. The difference between the estimate of δ_d and δ_c will be $\delta_d \approx \delta_c \cos\alpha$, where α is the angle of a tangent of the boundary curve relative to the mean camber line. This angle will be limited to a few degrees, and accordingly, the $\cos\alpha$ term will be sufficiently close to unity to allow for the approximation $\delta_d \approx \delta_c$. This means that the Delaunay triangulation can be used to find the mean camber line as an interpolation of the centers $\mathbf{q}_{ijk}$ of the circumcircle of the Delaunay triangles T_{ijk}.

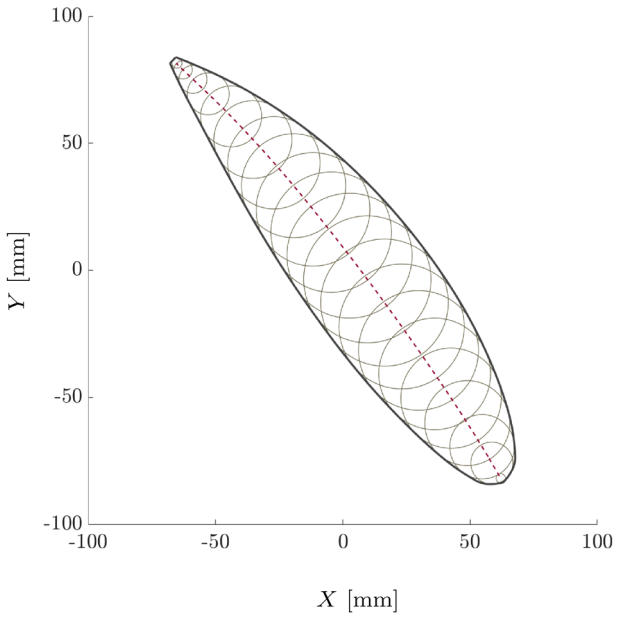

Fig. 11 The propeller blade section from Fig. 10 with a subset of the Delaunay triangulation circumcircles, in addition to the mean camber line identified via the circumcenters of the Delaunay triangles

It is noted that each Delaunay triangle T_{ijk} has three corners. In this case, two points will be on the suction side and one on the pressure side, or vice versa. This will not pose any problem as long as the points of the boundary curve are sufficiently close.

Figure 11 shows the computed Delaunay triangle circumcircles and the circle centers as an approximation of the mean camber line of the example propeller blade section. The corresponding Voronoi diagram is shown in Fig. 10.

3.5 Identification of edges and chord line

Close to the leading and trailing edges, reliable identification of the camber line and section thickness is challenging. The approach based on Voronoi diagrams and Delaunay triangulation forms a fork in the mean camber line at the section edges if the radius of the Delaunay triangle circumcircles is less than the edge radius, or if the trailing edge has sharp corners. As a consequence, the triangulation quality is dependent on the shape of the foil section edges. To overcome this difficulty while robustly identify the intersection of the section boundary with the mean camber line, we perform a least-squares fit of a small straight line segment at each end of the foil section

$$f_{\mathrm{LE}}(x) = a_{\mathrm{LE}}x + b_{\mathrm{LE}} \tag{21}$$

and

$$f_{\mathrm{TE}}(x) = a_{\mathrm{TE}}x + b_{\mathrm{TE}}, \tag{22}$$

with slope coefficients a_{LE} and a_{TE}, and intercept coefficients b_{LE} and b_{TE}. The coefficients are computed from subsets S_{LE}, $S_{\mathrm{TE}} \in S$ for each foil section. The subsets are selected by performing a k-nearest neighbor search at each end of the initial mean camber line, which is identified as described in the previous section. It is expected that the straight line segments sufficiently approximate the camber line at each end for small distances.

The points representing the leading edge p_{LE} and trailing edge p_{TE} can then be found from the intersections of the section boundary $K(l_a)$ with the best-fit straight lines $f_{\mathrm{LE}}(x)$ and $f_{\mathrm{TE}}(x)$, respectively.

The chord length l is found by computing the Euclidean distance between the leading and trailing edges $\mathbf{p}_{\mathrm{LE}}$ and $\mathbf{p}_{\mathrm{TE}}$. The notable sectional midpoint p_{M} originates as the bisection of the chord line, which is a line drawn between the leading and trailing edges. The relationships linking the chord length, chord line, sectional midpoint, and leading and trailing edges are shown in Fig. 9. The local pitch angle is found from the sectional midpoint $\mathbf{p}_{\mathrm{M}} = [p_{\mathrm{Mx}}, p_{\mathrm{My}}]^{\mathrm{T}}$ which is given by

$$\mathbf{p}_{\mathrm{M}} = \frac{\mathbf{p}_{\mathrm{LE}} + \mathbf{p}_{\mathrm{TE}}}{2}. \tag{23}$$

The local pitch angle is then computed from

$$\alpha = \arctan2(p_{\mathrm{My}}, p_{\mathrm{Mx}}). \tag{24}$$

From the parameters identified by the arrangements described in this and the previous sections, it is possible to derive the camber of the observed blade section as the maximal Euclidean distance between the sectional chord and camber lines.

4 Experimental results and discussion

The proposed approach for identifying geometric design parameters is validated by experiments performed on synthetic and real measured data. We demonstrate our procedure by identifying the design parameters of two marine propeller blades: a propulsion blade made from synthetically generated data, and a high-skew thruster blade of which we have

Table 1 Geometric propeller parameters for the KVLCC KP458 propeller as designed by MOERI

r/R	P/D	θ_s (°)	l/D	$\frac{f_0}{D}(10^3)$	$\frac{t_0}{D}(10^3)$	f_0/l
0.16	0.5765	− 2.53	0.1515	4.74	46.81	0.0313
0.25	0.6130	− 4.00	0.1772	6.18	42.17	0.0349
0.30	0.6310	− 4.40	0.1892	6.74	38.52	0.0356
0.40	0.6630	− 4.40	0.2093	7.08	32.02	0.0338
0.50	0.6915	− 3.15	0.2247	6.59	26.02	0.0293
0.60	0.7120	− 0.82	0.2335	5.83	20.55	0.0250
0.70	0.7212	2.49	0.2338	5.12	15.60	0.0219
0.80	0.7160	6.35	0.2192	4.34	11.05	0.0198
0.90	0.6927	10.76	0.1808	2.92	7.00	0.0161
0.95	0.6748	13.15	0.1422	1.82	4.72	0.0128
1.00	0.6510	16.75	0.0000	0.05	3.20	3.0625

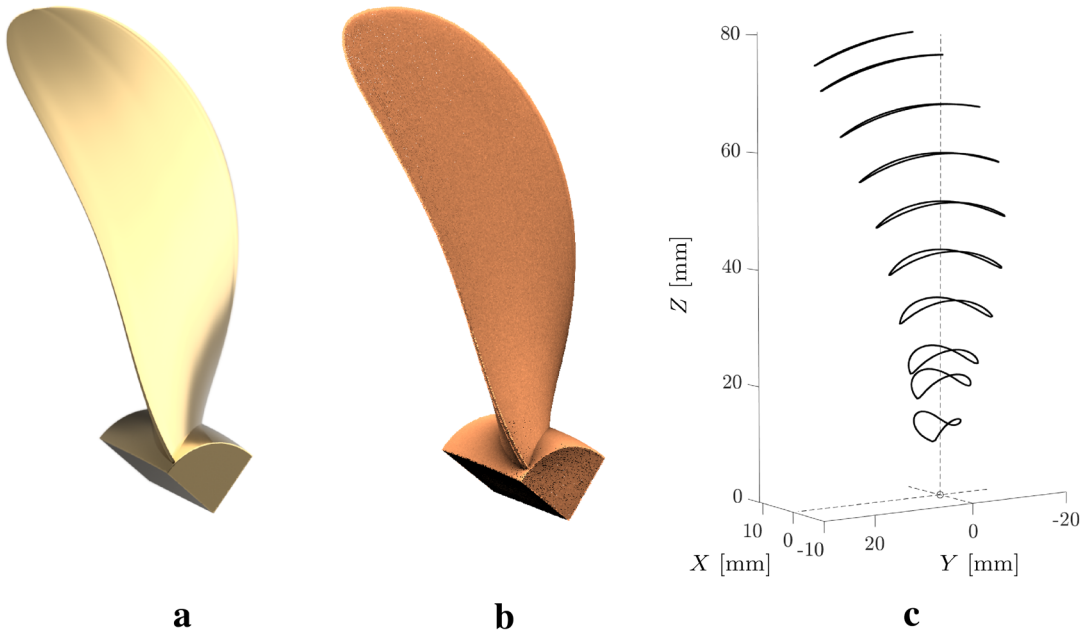

Fig. 12 CAD model of a section of the KP458 propeller (**a**). A point cloud randomly sampled on the surface of the KP458 model (**b**). The extracted radial sections are shown in **c**

performed 3D scans and CMM measurements. We primarily consider two aspects when analyzing the performance, which is the geometrical shape error and its sensitivity to noisy measurements.

4.1 MOERI tanker KVLCC2

To test our approach on a model where ground-truth design parameters exist, we chose to use a cloud of points sampled from a commonly studied and available propeller model. The KRISO Very Large Crude Carrier 2 (KVLCC2) is a tanker designed by the Maritime Ocean Engineering Research Institute in Korea (MOERI). The design model was formed in 1997 to investigate the explication of flow physics and performing CFD validations on a 300,000 tons deadweight (DWT) tanker ship. No full-scale embodiment of the ship exists.

The KVLCC2 is appended with a 4-blade fixed-pitch propeller with a diameter of 9.86 m named KP458. This propeller model has been used in the testing of our approach, with a model scale of 1:58. Hence, the diameter of the scaled propeller model is 170 cm. The design parameters of the scaled propeller model are listed in Table 1.

To adequately mimic point cloud data originating from 3D scanning, we randomly distribute a set of points over one

Table 2 Geometric propeller parameters for the KVLCC KP458 propeller identified via the proposed approach

r/R	P/D	θ_s (°)	l/D	$\frac{f_0}{D}(10^3)$	$\frac{t_0}{D}(10^3)$	f_0/l
0.16	0.5783	− 2.63	0.1529	4.83	46.61	0.0316
0.25	0.6130	− 3.99	0.1772	6.19	42.15	0.0349
0.30	0.6310	− 4.39	0.1892	6.74	38.50	0.0357
0.40	0.6631	− 4.39	0.2093	7.08	32.00	0.0338
0.50	0.6916	− 3.14	0.2247	6.59	26.00	0.0294
0.60	0.7121	− 0.82	0.2335	5.84	20.54	0.0250
0.70	0.7213	2.49	0.2338	5.12	15.59	0.0219
0.80	0.7161	6.33	0.2191	4.34	11.04	0.0198
0.90	0.6928	10.64	0.1808	2.92	6.99	0.0162
0.95	0.6749	12.93	0.1420	1.82	4.74	0.0128
1.00	–	–	–	–	–	–

Table 3 Geometric absolute errors for parameter identification of the KP458 propeller

	Mean	SD	Min	Max
P/D	0.0003	0.0006	0.0000	0.0018
θ_s (°)	0.0500	0.0742	0.0025	0.2229
l/D	0.0002	0.0004	0.0000	0.0014
f_0/D(10^3)	0.0121	0.0287	0.0002	0.0934
t_0/D(10^3)	0.0350	0.0596	0.0066	0.2037
f_0/l	0.0001	0.0001	0.0000	0.0003

The errors are computed as the arithmetic mean, sample standard deviation, and minimum and maximum absolute deviations

of the propeller model blades. More precisely, 10 million points are sampled on a surface representation of the model embodied as unstructured triangles [25]. On the resulting unorganized point cloud, the approach for parameter identification is conducted as described in Sect. 3. Figure 12 shows the surface representation of a KP458-blade, along with a point cloud representation of the blade made in the sampling step. The figure also illustrates the first step of our procedure, where the 0.16R, 0.25R, 0.30R, 0.40R, 0.50R, 0.60R, 0.70R, 0.80R, 0.90R, and 0.95R sections are extracted from the point cloud.

The resulting identified blade parameters for each radial section are listed in Table 2. An exception is the 1.0R-section located at the very tip of the blade. For this section, it is not practicable to extract a sufficient number of points, making meaningful retrieval of the geometric parameters a highly involved task. For the sections that were extracted and evaluated, the absolute geometric errors between the designed and identified parameters are given in Table 3. In Fig. 13, the identified propeller geometry parameters are compared with the design parameters. Additionally, the derived 0.7R-section of the KP458-blade is shown.

4.1.1 Noise tolerance

Point cloud data acquired from 3D sensors contain measurement uncertainty. Hence, the parameter identification procedure needs to be robust in the face of noisy data. To test our approach for various levels of measurement noise, we study the set of points S_N of points $\mathbf{p}_{Ni} = \mathbf{p}_i + \mathbf{E}_i$, $i = 1, \ldots, n$, where the additive noise $\mathbf{E}_i$ is used to mimic the uncertainly in real scanned depth data.

A wide range of depth sensors is commercially available at different levels of accuracy and costs. The additive noise $\mathbf{E}$ depends on the particulars of each sensor. As it is complex to define precise noise models for all sensors, we select a standard Gaussian noise model

$$\mathbf{E} \sim \mathcal{N}(0, \sigma^2 \mathbf{I}), \tag{25}$$

where $\mathbf{I}$ is the identity matrix, and the standard deviation of the noise is found from

$$\sigma^2 = \frac{\mu^T \mu}{\mathrm{SNR}} \quad \text{and} \quad \mu = \frac{1}{n} \sum_{i=0}^{n} \mathbf{p}_i \tag{26}$$

for a given signal-to-noise ratio (SNR) specified in dB. This model is commonly known as zero-mean additive white Gaussian noise (AWGN). Figure 14 illustrates how the tip of the KP458 propeller blade is influenced by the added noise at various levels: SNR = $\{40, 45, 50, 55, 60\}$. A higher SNR value implies less distortion of the point cloud. In Fig. 15, the design parameters of the propeller geometry are compared with the identified parameters for the various levels of additive noise. It is worth noting that additive noise with SNR of 45 dB and below would for the given amount of points and their extent correspond to unrealistic levels of noise when considering industrial 3D scanning systems. From the plots in Fig. 14, it can be seen that for the skew angle θ_s and thickness distribution t_0, the added noise has a

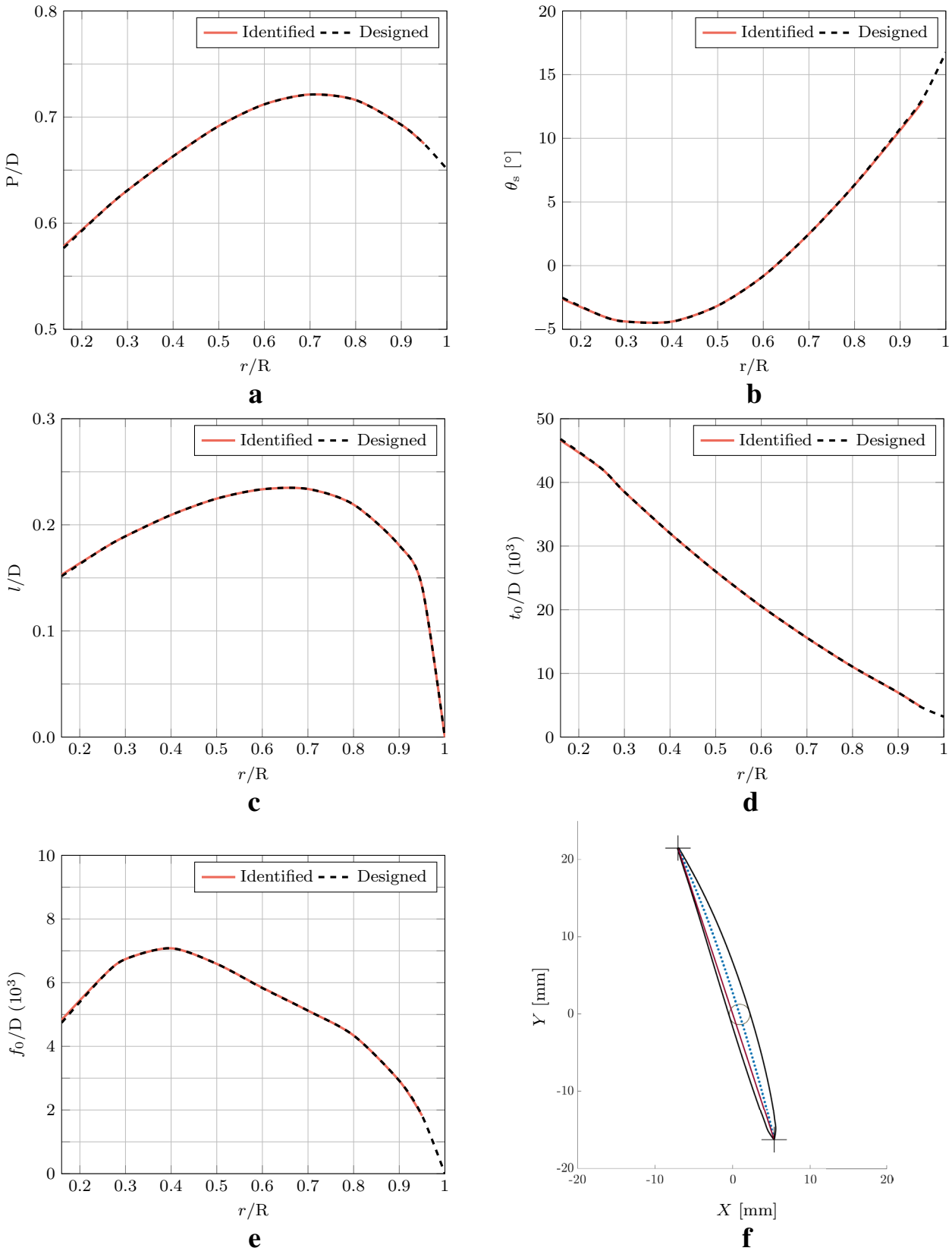

Fig. 13 Correspondence between identified and designed values for the various parameter distributions of the KP458 propeller model: **a** pitch; **b** skew angle; **c** chord length; **d** maximum thickness; **e** maximum camber. The 0.70R-section is shown in **f**, with markings of its mean camber line, chord line, maximum thickness, and leading and trailing edges

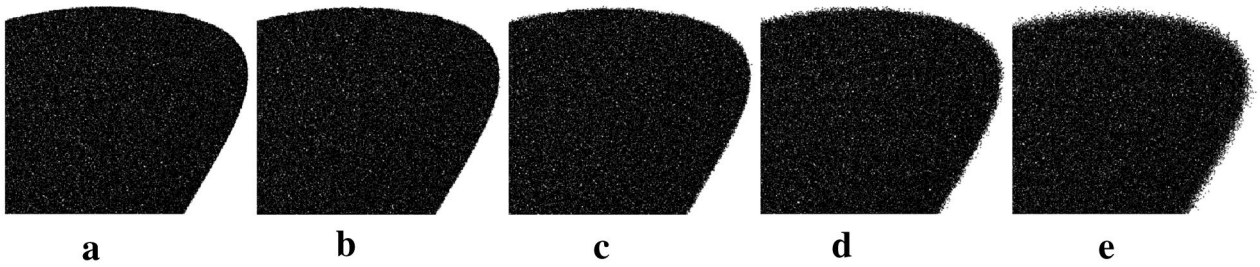

Fig. 14 Point cloud representation of the tip of the KVLCC KP458 propeller blade with increasing levels of additive Gaussian white noise added. **a** 60 dB, **b** 55 dB, **c** 50 dB, **d** 45 dB, and **e** 40 dB

relatively low influence. For the other parameters, the various levels of noise have a more significant but still modest influence. The effect is most evident for added noise with SNR below 50 dB.

4.2 3D scanning of a marine thruster blade

A second case study is provided to illustrate the capacities of the proposed approach when given real data originating from 3D scanning. The propeller blade examined in this experiment was designed for a four-blade, controllable pitch propeller cast in NiAl-Bronze. The total diameter of the propeller is 3600 mm, and the blade is right-handed with a propeller skew angle of 29°. Thus, it is categorized as a highly skewed propeller. It was manufactured following the tolerances in ISO 484-1:2015(E), for accuracy Class 1. The design parameters of the thruster blade are listed in Table 4.

The 3D scanning of the blade was conducted in a GOM ATOS Scanbox MV 700, where the scanning 3D camera uses the structured light principle. The system has a specified maximum point spacing of 0.213 mm within the measuring volume. During the acquisition, the edges and root of the blade were coated with micro-particle spray to improve the scanning performance. A photograph of the 3D scanning setup during execution is shown in Fig. 16a, with a rendering of the resulting scan of the propeller blade in Fig. 16b. A total of 4.9 million points were sampled on the blade surface.

Based on the acquired point cloud, we effectuated our suggested approach for parameter identification, as described in Sect. 3. In Table 5, the resulting identified geometric parameters are listed for each radial section. A prerequisite for using the thruster blade in an analysis of the proposed parameter identification method is that the blade has been made entirely to the exact tolerances. During manufacturing, several factors contribute to dimensional inaccuracies, resulting in product geometry that does not fully match the design parameters. Independent measurements of the blade geometry are hence required to evaluate the capabilities of the proposed method. In this regard, we conducted CMM measurements of the thruster blade surfaces for comparison. The blade pitch and thickness distribution were measured, and the results are shown in Table 6.

In Fig. 17, the identified geometry parameters of the thruster blade are compared with the design parameters and with CMM measurements where available. Additionally, the derived 0.7R-section of the blade is shown. For the sections that were extracted and evaluated, the absolute geometric errors between the designed and identified parameters and between identified parameters and CMM measurements are given in Table 7.

From the results obtained in this case study, it can be seen that the proposed approach is successful in identifying the pitch P, skew angle θ_s, chord length l, and maximum thickness t_0 of the thruster blade sections. The findings are, however, not as robust for the identification of camber distribution f_0. Although the deviations are within the specified manufacturing tolerances, it is worth noting that the camber parameter is highly dependent on accurate identification of the leading and trailing edges. Small deviations in locating the blade edges make a significant impact on the following determination of the maximum camber of the sections.

Another critical aspect concerning precise parameter identification for individual propeller and thruster blades is to ensure the correct orientation of the blade relative to its reference plane and axis, i.e., the datum of the blade. The thruster blade inspected in this case study was oriented according to its center and guiding holes. As for the leading and trailing edges, small deviations in the initial orientation of the blade make a significant impact on parameter identification. Precise orientation is of importance both for 3D scanning and for CMM measurements.

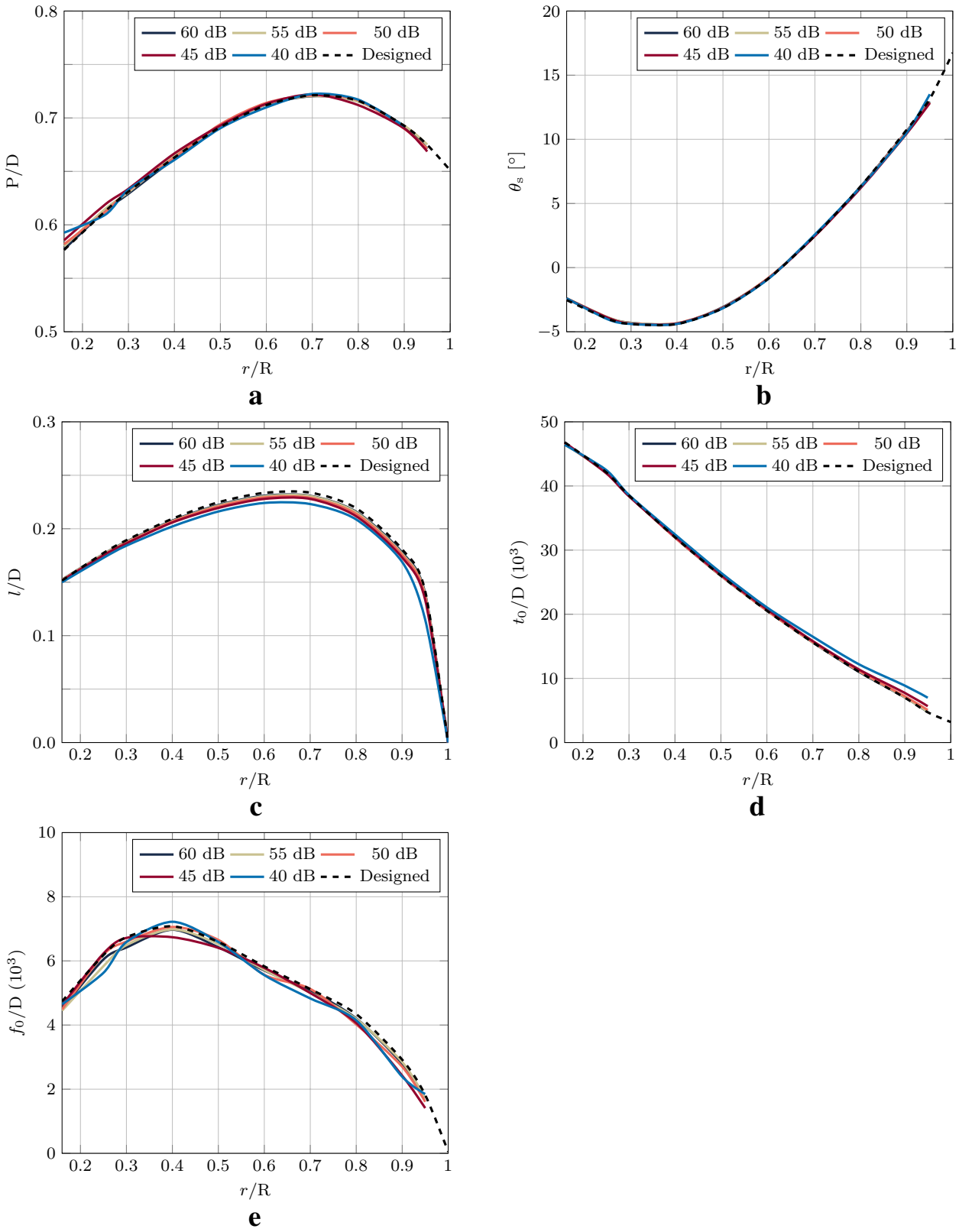

Fig. 15 Correspondence between identified and designed values for the various parameter distributions of the KP458 propeller model: **a** pitch; **b** skew angle; **c** chord length; **d** maximum thickness; **e** maximum camber

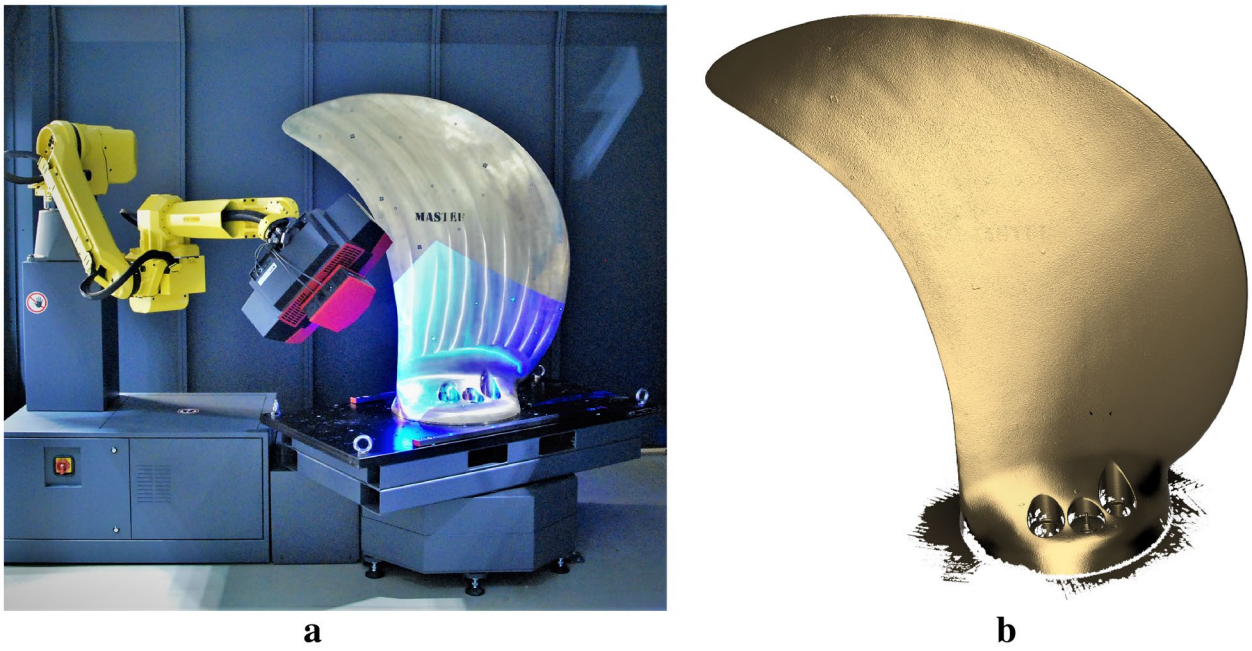

Fig. 16 **a** 3D scanning of the thruster blade in a GOM ATOS ScanBox. **b** The resulting 3D scan of the propeller blade

Table 4 Design propeller data for the thruster blade

r/R	P/D	θ_s (°)	l/D	$\frac{f_0}{D}(10^3)$	$\frac{t_0}{D}(10^3)$	f_0/l
0.40	0.910	35.91	0.1944	8.43	38.36	0.0434
0.50	0.938	30.84	0.2104	7.82	32.03	0.0372
0.60	0.951	26.77	0.2234	7.25	26.11	0.0324
0.70	0.963	23.65	0.2330	7.08	20.53	0.0304
0.80	0.961	20.93	0.2375	6.94	15.33	0.0292
0.90	0.913	17.90	0.2223	6.31	10.44	0.0284
0.95	0.853	15.95	0.1899	5.17	8.11	0.0272
1.00	–	–	–	–	–	–

Table 5 Identified propeller data for the thruster blade by the proposed approach

r/R	P/D	θ_s (°)	l/D	$\frac{f_0}{D}(10^3)$	$\frac{t_0}{D}(10^3)$	f_0/l
0.40	0.914	36.04	0.1950	8.14	37.85	0.0412
0.50	0.938	30.86	0.2103	7.65	31.91	0.0380
0.60	0.946	26.65	0.2238	7.14	26.10	0.0336
0.70	0.962	23.62	0.2330	7.02	20.60	0.0307
0.80	0.960	20.90	0.2386	6.93	15.42	0.0291
0.90	0.913	17.90	0.2225	6.12	10.36	0.0274
0.95	0.855	15.99	0.1940	5.10	8.32	0.0263
1.00	–	–	–	–	–	–

Table 6 CMM thickness and pitch measurements for the thruster blade

r/R	P/D	$\frac{t_0}{\mathrm{D}}(10^3)$
0.40	0.911	37.91
0.50	0.935	31.97
0.60	0.948	26.13
0.70	0.962	20.61
0.80	0.960	15.44
0.90	0.914	10.38
0.95	0.861	8.36
1.00	–	–

Table 7 Geometric absolute errors as the arithmetic mean, sample standard deviation, and minimum and maximum absolute deviations for the thruster blade

Reference	Parameter	Mean	SD	Min	Max
Design data	P/D	0.002	0.002	0.000	0.005
	θ_s	0.056	0.049	0.002	0.131
	l/D	0.001	0.001	0.000	0.004
	f_0/D(10^3)	0.244	0.183	0.010	0.484
	t_0/D(10^3)	0.155	0.166	0.007	0.507
	f_0/l	0.001	0.001	0.000	0.002
CMM	P/D	0.002	0.002	0.000	0.006
	t_0/D(10^3)	0.033	0.020	0.014	0.064

5 Summary and conclusions

In this work, we have presented a procedure for identifying the various geometric design parameters of marine propeller blades based on discrete point cloud data originating from 3D scanning. The proposed approach is based on extracting the radial sections from the scanned point cloud, and then extracting it to a planar surface where the foil parameters can be identified. A central contribution is the use of Voronoi diagrams and Delaunay triangulation for determining the mean camber line of each section robustly.

Experimental results from various case studies have demonstrated the effectiveness of the presented approach in extracting and identifying the chord line and mean camber line of the radial propeller foil sections. Consequently, the various geometric design parameters such as the pitch, chord length, skew, thickness, and camber distributions are identified. The presented method is shown to be robust to various levels of measurement uncertainty, and assumed a reliable method for extracting and analyzing the defining foil sections of marine propeller blades.

Future work will focus on practical applications of the suggested approach. Inspection, reconstruction, and parameter extraction are common problems in propeller blade manufacturing, and the proposed method can find several specific applications. We believe that the proposed method has the potential for successful application in the final inspection of manufactured marine propeller blades, in-line measurements in robotic grinding and surface finishing processes, and wear assessment or reverse engineering of propellers in service.

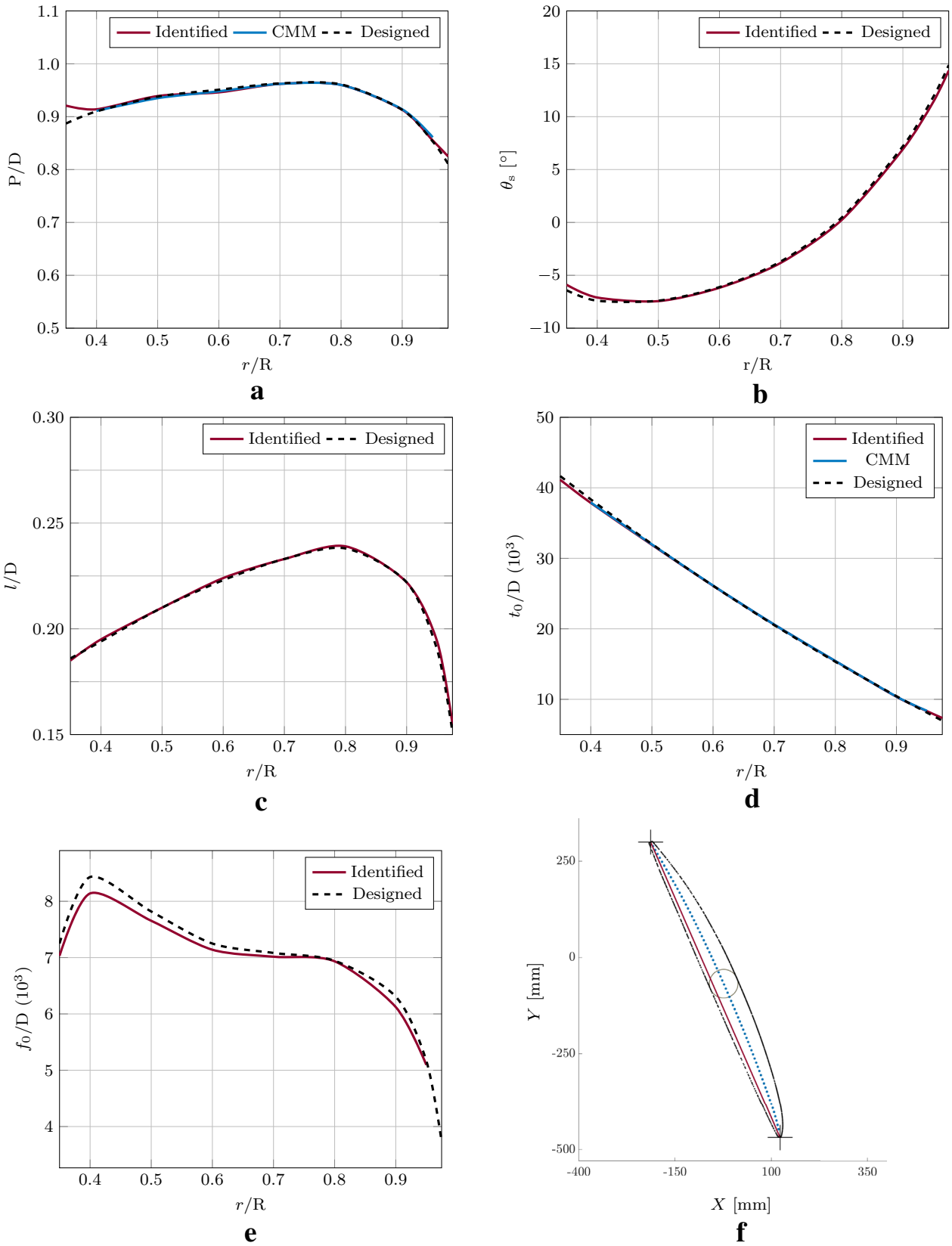

Fig. 17 Correspondence between identified and designed values for the various parameter distributions of the thruster blade: **a** Pitch; **b** skew angle; **c** chord length; **d** maximum thickness; **e** maximum camber. The 0.70R-section is shown in **f**, with markings of its mean camber line, chord line, maximum thickness, and leading and trailing edges

Acknowledgements The authors wish to thank the OLIVER project and industrial partner Oshaug Metall AS. Also, we would like to express great appreciation to Njaal H. Munthe-Kaas for his contributions to this work. The Norwegian Research Council supports the project under the BIA program, Project Number 261639.

Funding Open access funding provided by NTNU Norwegian University of Science and Technology (incl St. Olavs Hospital - Trondheim University Hospital).

References

1. Golini D (1991) Precision surfacing and metrology of naval propellers. In: Proceedings of the propellers 91 symposium Virgina Beach, Virginia, pp 3-1–3-6
2. Menna F, Troisi S (2010) Low cost reverse engineering techniques for 3D modelling of propellers. Int Arch Photogramm Remote Sens Spat Inf Sci 38(Part 5):452–457
3. Zhang J, Lu J (2011) Measuring propeller blade width using binocular stereo vision. J Mar Sci Appl 10(2):246–251
4. Abdullah AB, Salit MS, Samad Z, MTandoor KH, Aziz NA (2013) Twist springback measurement of autonomous underwater vehicle propeller blade based on profile deviation. Am J Appl Sci 10(5):515
5. Cavada J, Fadón F (2012) Application of laser technology for measurement and verification of marine propellers. In: ASME 2012 11th biennial conference on engineering systems design and analysis. American Society of Mechanical Engineers, pp 467–475
6. Yeo KB, Choong WH (2014) Marine propeller geometry characterization. J Appl Sci 14(23):3288–3293
7. Abbas MA, Lichti DD, Chong AK, Setan H, Majid Z, Lau CL, Idris KM, Ariff MFM (2017) Improvements to the accuracy of prototype ship models measurement method using terrestrial laser scanner. Measurement 100:301–310
8. Tassetti N, Martelli M, Buglioni G (2015) Reverse engineering techniques for trawler hull 3D modelling and energy efficiency evaluation. In: Proceedings of NAV 18th international conference on ships and shipping research. ATENA, Lecco, pp 24–26
9. Hand SD, Mongon WJ, Clark JF, Schindelholz E (2005) Measurement of the USS monitor propeller using structured light and coherent laser radar scanning technologies. In: Proceedings of the CMSC 2005 coordinate systems measurement conference
10. Khameneifar F, Feng H-Y (2017) Extracting sectional contours from scanned point clouds via adaptive surface projection. Int J Prod Res 55(15):4466–4480
11. Li W-L, Xie H, Li Q-D, Zhou L-P, Yin Z-P (2014) Section curve reconstruction and mean-camber curve extraction of a point-sampled blade surface. PLoS One 9(12):e115471
12. Mohaghegh K, Sadeghi M, Abdullah A (2007) Reverse engineering of turbine blades based on design intent. Int J Adv Manuf Technol 32(9–10):1009–1020
13. Li W-L, Xie H, Zhang G, Yan S-J, Yin Z-P (2016) 3-D shape matching of a blade surface in robotic grinding applications. IEEE/ASME Trans Mechatron 21(5):2294–2306
14. Patrikalakis NM, Bardis L (1992) Feature extraction from B-spline marine propeller representations. J Ship Res 36(3):233–247
15. Jinkerson RA, Abrams SL, Bardis L, Chryssostomidis C, Clément A, Patrikalakis NM, Wolter F-E (1993) Inspection and feature extraction of marine propellers. J Ship Prod 9:88–88
16. Allen DW, Howell IL, McIntyre CJ, Reiser JJ, Machin JD, Hettema CD, Madden CJ (2005) Propeller geometric parameter extraction from inspection data clouds. J Ship Prod 21(4):203–208
17. Li W, Xu S, Zhao G, Goh LP (2005) Adaptive knot placement in b-spline curve approximation. Comput Aided Des 37(8):791–797
18. Kostas K, Amiralin A, Sagimbayev S, Massalov T, Kalel Y, Politis C (2020) Parametric model for the reconstruction and representation of hydrofoils and airfoils. Ocean Eng 199:107020
19. Masters DA, Taylor NJ, Rendall T, Allen CB, Poole DJ (2017) Geometric comparison of aerofoil shape parameterization methods. AIAA J 55(5):1575–1589
20. Arapakopoulos A, Polichshuk R, Segizbayev Z, Ospanov S, Ginnis A, Kostas K (2019) Parametric models for marine propellers. Ocean Eng 192:106595
21. Carlton J (2018) Marine propellers and propulsion. Butterworth-Heinemann, Oxford
22. de Berg M, Cheong O, van Kreveld M, Overmars M (2008) Computational Geometry. Algorithms and Applications, 3rd edn. Springer, Berlin
23. Aurenhammer F (1991) Voronoi diagrams—a survey of a fundamental geometric data structure. ACM Comput Surv (CSUR) 23(3):345–405
24. Lee D-T, Schachter BJ (1980) Two algorithms for constructing a Delaunay triangulation. Int J Comput Inf Sci 9(3):219–242
25. Turk G (1990) Generating random points in triangles. In: Glassner AS (ed) Graphics gems. Academic Press Professional, San Diego, pp 24–28